



## Combined shape and topology optimization of 3D structures

**Christiansen, Asger Nyman; Bærentzen, Jakob Andreas; Nobel-Jørgensen, Morten; Aage, Niels; Sigmund, Ole**

*Published in:*  
Computers & Graphics

*Link to article, DOI:*  
[10.1016/j.cag.2014.09.021](https://doi.org/10.1016/j.cag.2014.09.021)

*Publication date:*  
2015

*Document Version*  
Peer reviewed version

[Link back to DTU Orbit](#)

*Citation (APA):*  
Christiansen, A. N., Bærentzen, J. A., Nobel-Jørgensen, M., Aage, N., & Sigmund, O. (2015). Combined shape and topology optimization of 3D structures. *Computers & Graphics*, 46, 25-35.  
<https://doi.org/10.1016/j.cag.2014.09.021>

---

### General rights

Copyright and moral rights for the publications made accessible in the public portal are retained by the authors and/or other copyright owners and it is a condition of accessing publications that users recognise and abide by the legal requirements associated with these rights.

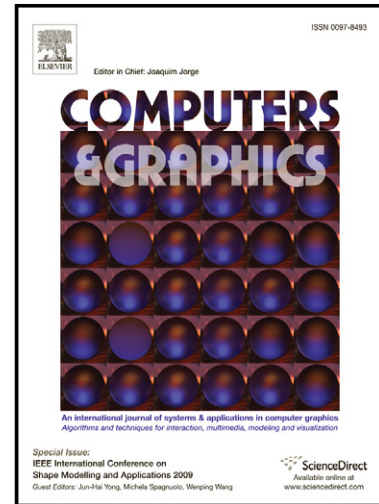
- Users may download and print one copy of any publication from the public portal for the purpose of private study or research.
- You may not further distribute the material or use it for any profit-making activity or commercial gain
- You may freely distribute the URL identifying the publication in the public portal

If you believe that this document breaches copyright please contact us providing details, and we will remove access to the work immediately and investigate your claim.

# Author's Accepted Manuscript

Combined shape and topology optimization of  
3D structures

Asger N. Christiansen, J. Andreas Bærentzen,  
Morten Nobel-Jørgensen, Niels Aage, Ole  
Sigmund



PII: S0097-8493(14)00109-5  
DOI: <http://dx.doi.org/10.1016/j.cag.2014.09.021>  
Reference: CAG2511

To appear in: *Computers & Graphics*

Received date: 29 June 2014  
Revised date: 24 August 2014  
Accepted date: 16 September 2014

Cite this article as: Asger N. Christiansen, J. Andreas Bærentzen, Morten Nobel-Jørgensen, Niels Aage, Ole Sigmund, Combined shape and topology optimization of 3D structures, *Computers & Graphics*, <http://dx.doi.org/10.1016/j.cag.2014.09.021>

This is a PDF file of an unedited manuscript that has been accepted for publication. As a service to our customers we are providing this early version of the manuscript. The manuscript will undergo copyediting, typesetting, and review of the resulting galley proof before it is published in its final citable form. Please note that during the production process errors may be discovered which could affect the content, and all legal disclaimers that apply to the journal pertain.

# Combined Shape and Topology Optimization of 3D Structures

Asger N. Christiansen, J. Andreas Bærentzen, Morten Nobel-Jørgensen, Niels Aage, Ole Sigmund

*Technical University of Denmark, Denmark*

## Abstract

We present a method for automatic generation of 3D models based on shape and topology optimization. The optimization procedure, or model generation process, is initialized by a set of boundary conditions, an objective function, constraints and an initial structure. Using this input, the method will automatically deform and change the topology of the initial structure such that the objective function is optimized subject to the specified constraints and boundary conditions. For example, this tool can be used to improve the stiffness of a structure before printing, reduce the amount of material needed to construct a bridge, or to design functional chairs, tables, etc. which at the same time are visually pleasing.

The structure is represented explicitly by a simplicial complex and deformed by moving surface vertices and re-labeling tetrahedra. To ensure a well-formed tetrahedral mesh during these deformations, the Deformable Simplicial Complex method is used. The deformations are based on optimizing the objective, which in this paper will be maximizing stiffness. Furthermore, the optimization procedure will be subject to constraints such as a limit on the amount of material and the difference from the original shape.

*Keywords:* Topology optimization, shape optimization, Deformable Simplicial Complex method, structural design

## 1. Introduction

Topology optimization is the discipline of finding the optimal shape and topology of a structure [1][2]. It can be used to solve a wide variety of design problems arising when producing such diverse products as cars, houses, computer chips and antennas. The manufacturers are often concerned with finding the stiffest structure, the lightest structure which does not break, the structure with the highest cooling effect, or the structure with the best flow or highest efficiency.

With the advances in 3D printing technology, topology optimization is not just of interest to manufacturers, but to anyone who has access to a 3D printer. Most consumers lack formal training in structural mechanics, which can hinder the process with many iterations and costly failed attempts. Consumers can under-engineer a design unsuitable for the intended load, or over-engineer a design that wastes expensive construction material. Topology optimization offers consumers a tool for designing shapes that meet their structural needs while using minimal construction resources.

In this paper, we present a fully automated design tool for designing structurally sound structures which can be manufactured, constructed or printed. The modeler only

has to specify boundary conditions, the optimization objective, constraints and an initial structure. In other words, the designer specifies a set of requirements (the functionality of the structure and not the structure itself) and the method automatically designs a structure which fits those requirements. Note that this design process is significantly different from today where a designer manually models a structure and requirements are taken into account during this design process.

The proposed method for topology optimization is based on the Deformable Simplicial Complex (DSC) method [3]. The DSC method represents a solid structure with a conforming tetrahedral mesh (a simplicial complex) whose tetrahedral elements either lie entirely inside or outside the structure. The interface between solid and void (the surface) is represented explicitly by the triangular faces shared by an interior and exterior tetrahedral element. Furthermore, the DSC method ensures well-formed tetrahedral elements by constantly performing mesh improvement routines while the surface is being deformed. Finally, it provides adaptive resolution, allowing fine details where and when needed.

The method uses two optimization strategies:

### 48 *Discrete optimization*

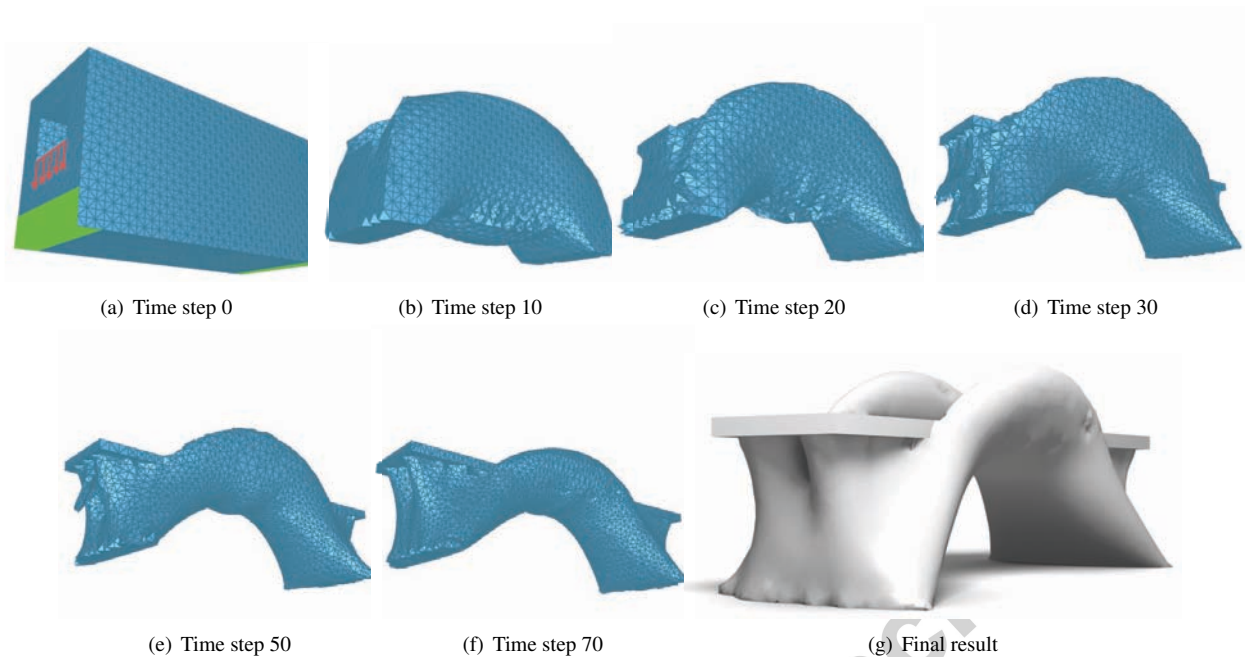


Figure 1: Given a few input parameters, the proposed method automatically optimizes the shape and topology of a 3D structure. Here is an example of optimizing a bridge. The initial structure is seen to the upper left along with supports (green) and loads (red). This structure is optimized such that stiffness is maximized and the amount of material is minimized. A few iterations of the method are depicted along with the result.

49 Relabels elements from solid to void to improve  
 50 the objective or constraints which are not satisfied.  
 51 The relabeling is based on topological derivatives  
 52 [4][5][6][7][8], i.e. the change in the objective or  
 53 constraints by introducing an infinitesimal hole.

#### 54 *Continuous optimization*

55 Performs a non-parametric shape optimization  
 56 [9][10][11][12][13]. First, an improved shape,  
 57 which is within a small perturbation of the current  
 58 shape, is found by solving a constrained optimization  
 59 problem using the Method of Moving Asymptotes  
 60 (MMA) [14]. The surface is then deformed  
 61 to this improved shape using the DSC method [3].  
 62 While the surface is deformed, the mesh is adapted  
 63 such that its tetrahedral elements are well-formed  
 64 at all times.

65 These optimization strategies are iterated until changes  
 66 are small. An example is seen in Figure 1.

67 We will show that this tool is of interest to both engi-  
 68 neers and designers. For example, we show that it can  
 69 be used to improve stiffness and balance of a 3D model,  
 70 to save material and to generate functional as well as, in  
 71 our opinion, visually pleasing designs.

#### 72 *1.1. Related work*

73 Recent trends in the computer graphics society are to  
 74 add mechanical properties to 3D models. Prévost et al.  
 75 have been concerned with the balance of printed models  
 76 [15], Skouras et al. about printing deformable characters  
 77 using a stiff and soft material [16] and several research  
 78 teams have focused on self-supporting masonry struc-  
 79 tures [17][18][19].

80 A major concern has been to improve the stiffness of  
 81 3D models. Umetani et al. perform a cross-sectional  
 82 structural analysis and visualize the result [20]. A user  
 83 can then manually edit the model to improve the stiff-  
 84 ness while getting almost instant feedback. The instant  
 85 feedback is only possible because the analysis is limited  
 86 to cross-sections. Stava et al. presents a more automated  
 87 method for improving stiffness [21]. They perform a  
 88 complete worst-case structural analysis on a tetrahedral  
 89 mesh to determine the structurally weak regions. Based  
 90 on this analysis, it is decided whether to improve the  
 91 model by thickening, hollowing or adding a strut. Fi-  
 92 nally, Zhou et al. [22] also perform a worst-case struc-  
 93 tural analysis with more precise determination of the  
 94 worst-case loads than in [21]. Furthermore, they con-  
 95 clude that solving a shape optimization problem to min-  
 96 imize stress is impractical due to the non-linearity and

97 non-convexity of the problem. Therefore, they make do  
98 with visualizing the structurally weak regions.

99 Topology optimization problems are indeed non-  
100 convex. However, the topology optimization commu-  
101 nity has been solving these problems to at least local  
102 optimality for decades and the resulting designs usu-  
103 ally perform better than designs optimized by humans  
104 [2]. Feasible solutions to these problems are often found  
105 by standard numerical gradient-based optimization al-  
106 gorithms. However, note that the smooth compliance  
107 functional is often chosen as the objective function to  
108 ease the optimization instead of the non-smooth, but of-  
109 ten more interesting, maximal stress as Zhou et al. pro-  
110 pose.

111 A key ingredient in a topology optimization method  
112 is the shape representation which is required to be able  
113 to handle topology changes. Hence, topological opti-  
114 mization has focused primarily on implicit representa-  
115 tions over uniform voxel grids. Such representations  
116 can handle topology changes but lead to fixed-resolution  
117 results with cuberille artifacts. The most popular im-  
118 plicit topology optimization approaches are the density  
119 and level set approaches. The density approach [23][2]  
120 represents the structure by assigning a density value be-  
121 tween 0 (void) and 1 (material) to each cell in a fixed  
122 grid or mesh. The structure is now deformed by chang-  
123 ing these density values. The level set approach uses  
124 the level set method [24] evaluated on a fixed grid or  
125 mesh [25][26]. Here, the structure is represented by the  
126 zero level set and deformed by changes to the level set  
127 function. Both methods iteratively change the shape to  
128 approach the optimum.

129 We propose to represent the surface explicitly. An ex-  
130 plicit representation, for example a triangle mesh, has  
131 previously been used for shape optimization [9][10].  
132 However, shape optimization does not allow for topol-  
133 ogy changes and often only small shape deformations.  
134 Furthermore, it has been used in combination with the  
135 level set method [27][28][29][30][31] where it is neces-  
136 sary to constantly switch between the implicit and ex-  
137 plicit representations. An explicit representation has  
138 also been used in combination with a computationally  
139 expensive remeshing of the entire design domain at each  
140 iteration [4][32]. Finally, it has previously been shown  
141 that using the DSC method for topology optimization  
142 works in 2D and therefore has potential [33]. However,  
143 here, we show that this concept is able to solve real-  
144 world topology optimization problems in 3D.

145 Note that this list of structural optimization methods  
146 is far from exhaustive.

## 147 1.2. Contributions

148 The main contributions of this paper are as follows.

- 149 • As opposed to previous methods introduced in  
150 computer graphics, our method automatically opti-  
151 mizes the shape and topology of a structure given  
152 boundary conditions, an objective function, con-  
153 straints and an initial shape. This completely elimi-  
154 nates the manual editing which has been charac-  
155 teristic for the current approaches.
- 156 • Compared to current methods from the topology  
157 optimization community, the method uses a sin-  
158 gle explicit representation to represent the struc-  
159 ture and, at the same time, is able to handle topol-  
160 ogy changes. This gives rise to several advantages  
161 including a single mesh for shape representation  
162 and finite element calculations, possibility of both  
163 continuous and discrete optimization strategies and  
164 both the initial and optimized structure are in the  
165 form of surface triangle meshes. Finally, the adap-  
166 tive mesh makes it possible to achieve a much more  
167 detailed result within reasonable time on an ordi-  
168 nary laptop than otherwise possible using the stan-  
169 dard fixed grid methods.
- 170 • To be able to solve real-world topology optimiza-  
171 tion problems in 3D, it was necessary to make  
172 significant changes compared to the 2D proof-of-  
173 concept by Christiansen et al. [33]. Consequently,  
174 the discrete step relabels elements based on an op-  
175 timization procedure which takes constraints into  
176 account instead of based on a simple threshold of  
177 the objective. Furthermore, the presented method  
178 handles self weight, it is initialized by any surface  
179 triangle mesh, areas can be fixed to either solid  
180 or void and several global constraints have been  
181 implemented and utilized. Finally, the require-  
182 ments for computational efficiency is much higher  
183 in 3D than 2D. Therefore, the mesh adaptivity of  
184 the DSC method is utilized and the computations  
185 are distributed on multiple cores.

## 186 2. Method

187 The proposed method uses a simplicial complex to  
188 represent the shape of a structure. A simplicial com-  
189 plex discretizes a domain into tetrahedral elements. In  
190 3D it consists of the simplices; nodes (points), edges  
191 (line pieces), faces (triangles) and tetrahedra (triangular  
192 pyramids). Furthermore, the tetrahedra do not overlap  
193 and any point in the discretized domain is either inside

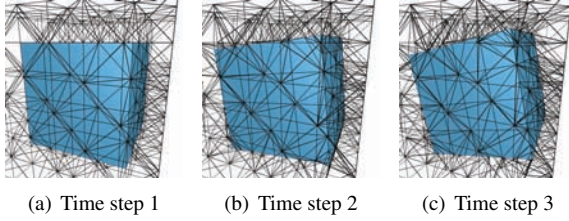


Figure 2: Rotation of a cube using the Deformable Simplicial Complex method. The interface between solid and void (the surface of the cube) is depicted in turquoise. Furthermore, all edges of the simplicial complex are drawn in black.

194 a tetrahedron or on the boundary between tetrahedra. In  
 195 addition, all tetrahedra are labeled as being either void  
 196 (no material) or solid (filled with material). Therefore,  
 197 the interface between solid and void (the surface) is rep-  
 198 resented by the faces that are sandwiched between a  
 199 tetrahedron labeled void and a tetrahedron labeled solid.  
 200 Figure 2 depicts a cube represented by a simplicial com-  
 201 plex. The tetrahedral mesh generator TetGen [34] is  
 202 used to generate the initial mesh.

203 Apart from the shape representation, the tetrahedral  
 204 elements of the simplicial complex can be used for  
 205 physical computations using the finite element method.  
 206 Since the finite element analysis will produce large er-  
 207 rors if used with nearly degenerate tetrahedra, it is im-  
 208 portant to sustain a high quality mesh.

### 209 2.1. Deformable Simplicial Complex method

210 To ensure a high quality mesh, we use the De-  
 211 formable Simplicial Complex (DSC) method [3]<sup>1</sup>. The  
 212 DSC method ensures high quality tetrahedral elements  
 213 during deformation of a model embedded in a simplicial  
 214 complex as illustrated in Figure 2. Low quality tetra-  
 215 hedra (slivers, wedges, caps and needles) are removed  
 216 by continuously performing a set of mesh operations  
 217 while the surface is being deformed. The tetrahedron  
 218 quality measure is  $\frac{6\sqrt{2}V}{(\frac{1}{6}\sum_i l_i^2)^{3/2}}$  [35] where  $V$  is the volume  
 219 of the tetrahedron and  $l_i$  is the length of edge  $i$ . Note  
 220 that the DSC method only improves the mesh quality  
 221 where necessary (often near the surface). Furthermore,  
 222 the DSC method also handles topology changes by re-  
 223 moving low quality tetrahedra which are sandwiched  
 224 between two surfaces. This is illustrated by two objects  
 225 colliding in Figure 3.

<sup>1</sup>An open-source framework is available at [www.github.com/asny/DSC](http://www.github.com/asny/DSC)

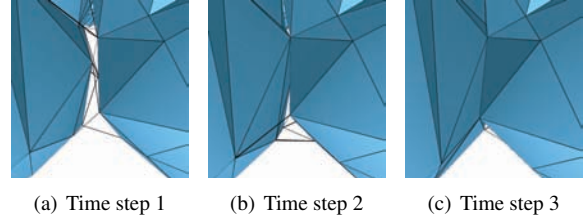


Figure 3: Illustration of topology changes using the Deformable Simplicial Complex method. Here, only edges having both end nodes on the surface are drawn. As the objects approach each other the tetrahedra between the objects get squeezed. When a tetrahedron between the two surfaces is squeezed too much, this tetrahedron will be collapsed. Consequently, the only thing separating the two objects is a face. However, this face has tetrahedra which are labeled solid on both sides and it is therefore no longer part of the surface. Consequently, the two objects are now merged into one.

226 In addition to ensuring high quality tetrahedral ele-  
 227 ments, the DSC method also controls the level of detail  
 228 of both the surface and the tetrahedral mesh. In prac-  
 229 tice, the DSC method attempts to collapse too small  
 230 simplices and split too large simplices. Consequently,  
 231 we always attain a mesh of the desired complexity, de-  
 232 scribed by the discretization parameter  $\delta$  (corresponding  
 233 to the average edge length). More importantly, the de-  
 234 tail control allows for mesh adaptivity. This means that  
 235 smooth regions on the surface are represented by a more  
 236 coarse discretization than regions with small features.

237 The mesh operations used are *smoothing* [36] (not  
 238 performed on surface nodes), *edge split* [37], *edge col-*  
 239 *lapse* [37], *edge removal* [38] and *multi-face removal*  
 240 [38]. The latter two use the flips illustrated in Figure  
 241 4. Consequently, these two mesh operations do not  
 242 change the position of any nodes, only the connectiv-  
 243 ity. The quality of the mesh is improved by all five  
 244 operations, whereas the detail level of the mesh is con-  
 245 trolled through the operations edge split and edge col-  
 246 lapse. Note that changes have been made compared to  
 247 [3]. The multi-face retriangulation, optimization-based  
 248 smoothing, null-space smoothing and tetrahedron rela-  
 249 beling operations have not been necessary for this ap-  
 250 plication. Removing these operations has resulted in a  
 251 significant speed-up. Also, the edge removal operation  
 252 on the surface and boundary is an addition since [3].

253 The strategy for moving the surface nodes is to first  
 254 compute a destination  $p_n^*$  for each surface node  $n$  cur-  
 255 rently at position  $p_n$ . The destination  $p_n^*$  is computed us-  
 256 ing a user-defined velocity function which, for the case  
 257 of topology optimization, will be described later. After-  
 258 wards, all surface nodes are moved from  $p_n$  to  $p_n^*$  us-  
 259 ing the strategy illustrated in Figure 5.

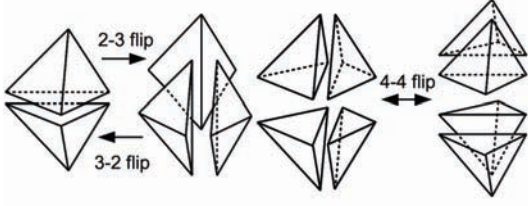


Figure 4: Illustrations of 2-3, 3-2 and 4-4 flips inspired by the illustration in [38].

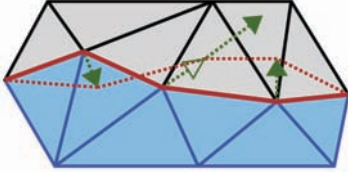


Figure 5: Illustration of how the surface (red) is moved in 2D. The same principle applies to 3D. A filled arrow indicates the destination  $\mathbf{p}_n^T$  of the surface node  $n$ . One of the nodes cannot move to its destination without creating low quality tetrahedra and it is therefore only moved as depicted by the unfilled arrow. The other two are moved to their destinations. Then, mesh operations are applied to improve the mesh quality and the node that did not reach its destination is moved again. This is repeated until all nodes have reached their destinations.

## 2.2. Structural analysis

In this paper, we will optimize the topology of physically valid structures in static equilibrium. In order to achieve physical validity, structural analyses using the finite element method are performed. This implies considering the *discretization, boundary conditions and equilibrium* which are the topics of this section.

As described previously, a domain is discretized into high quality tetrahedral elements which are analyzed using the finite element method. Using quadratic basis functions solves a well-known issue with a jagged surface when using the analysis as a basis for non-parametric shape optimization [11][12]. Consequently, quadratic basis functions are chosen instead of linear to interpolate the tetrahedral elements. Therefore one control point  $c$  is associated with each node and edge of a tetrahedron. Furthermore, the positions of all control points are assembled in a vector termed  $\mathbf{p} = [\dots, \mathbf{p}_c^T, \dots]^T$ . In addition, each tetrahedron  $t$  has an associated material  $m_t$  with material parameters *density*  $\rho_t$ , *Young's modulus*  $E_t$  and *Poisson's ratio*  $\nu_t$ . Finally, the materials of the tetrahedra are also assembled in a vector  $\mathbf{m} = [\dots, m_t, \dots]^T$ .

The local *stiffness matrix*  $\mathbf{K}_t$  contains information on the stiffness of tetrahedron  $t$ . It depends on both the positions of the control points  $\mathbf{p}$  and the materials of the

tetrahedra  $\mathbf{m}$  and can be calculated by

$$\mathbf{K}_t(\mathbf{m}, \mathbf{p}) = \int_{V_t} \mathbf{B}_t^T(\mathbf{p}) \mathbf{E}_t(\mathbf{m}) \mathbf{B}_t(\mathbf{p}) \partial(x, y, z) \quad (1)$$

We have chosen only to consider isotropic linear materials. Consequently, the constitutive matrix  $\mathbf{E}_t(\mathbf{m})$  which relates stress and strain is

$$\mathbf{E} = \frac{E}{(1+\nu)(1-2\nu)} \begin{bmatrix} 1-\nu & \nu & \nu & 0 & 0 & 0 \\ \nu & 1-\nu & \nu & 0 & 0 & 0 \\ \nu & \nu & 1-\nu & 0 & 0 & 0 \\ 0 & 0 & 0 & \frac{1-2\nu}{2} & 0 & 0 \\ 0 & 0 & 0 & 0 & \frac{1-2\nu}{2} & 0 \\ 0 & 0 & 0 & 0 & 0 & \frac{1-2\nu}{2} \end{bmatrix}$$

where  $\mathbf{E}_t(\mathbf{m})$  is shortened to  $\mathbf{E}$ ,  $E_t(\mathbf{m})$  to  $E$  and  $\nu_t(\mathbf{m})$  to  $\nu$ . Finally, the strain-displacement matrix  $\mathbf{B}_t(\mathbf{p})$  is related to the shape of the tetrahedron and the basis functions. For more details, see a text book on the finite element method used for structural analysis, e.g. [39]. The global stiffness matrix  $\mathbf{K}(\mathbf{m}, \mathbf{p})$  can then be assembled from the local stiffness matrices  $\mathbf{K}_t(\mathbf{m}, \mathbf{p})$ . Note that for elements with void as the associated material,  $\mathbf{K}_t$  is not defined. Consequently, the void elements are eliminated from the finite element analysis, which decreases computation time.

In this paper, we will limit ourselves to static problems subject to a single load case. These problems are modeled by supports and external forces  $\mathbf{f}_c$  which are both applied to the surface of the structure. In addition to external forces, the weight of the structure will cause gravitational forces

$$\mathbf{w}_c(\mathbf{m}, \mathbf{p}) = \mathbf{g} \sum_{i \in c} a_i \rho_i(\mathbf{m}) V_i(\mathbf{p}) \quad (2)$$

Here,  $\mathbf{g} = [0, -9.8, 0]^T m/s^2$  is a vector of the gravitational acceleration and  $a_i$  is a scale factor computed by a mass lumping scheme for each element  $i$ . Furthermore,  $\rho_i$  is the density and  $V_i(\mathbf{p})$  is the volume of tetrahedral element  $i$  which is adjacent to control point  $c$ . Consequently, the global *force vector* is

$$\mathbf{f}(\mathbf{m}, \mathbf{p}) = [\dots, \mathbf{f}_c^T + \mathbf{w}_c^T(\mathbf{m}, \mathbf{p}), \dots]^T \quad (3)$$

Since we desire a structure in static equilibrium, the sum of the forces on all particles must be zero (Newton's first law). Consequently, we will utilize the equilibrium equations

$$\mathbf{K}(\mathbf{m}, \mathbf{p}) \mathbf{u} = \mathbf{f}(\mathbf{m}, \mathbf{p}) \quad (4)$$

These equations are used to calculate the global *displacement vector*  $\mathbf{u} = [\dots, \mathbf{u}_c, \dots]$ . At each control

point  $c$ ,  $\mathbf{u}_c$  represents the displacement caused by the forces  $\mathbf{f}$  applied to the structure. Note that, since  $\mathbf{K}$  and  $\mathbf{f}$  are functions of  $\mathbf{p}$  and  $\mathbf{m}$ , so is  $\mathbf{u}$ .

Solving the equilibrium equations is the most time consuming part of the optimization. Furthermore, the number of equations scales linearly with the number of degrees of freedom. Consequently, the sparse solver *CHOLMOD* [40], which is a part of the *SuiteSparse* library [41], is used to solve the equilibrium equation efficiently using multiple cores.

### 2.3. Optimization

We want to optimize an objective function  $f$  by changing the shape and topology of the structure. Therefore, the objective can be anything as long as it is a function of the shape and topology. Furthermore, there are two ways to change the shape and topology. The first is to change the position  $\mathbf{p}_n$  of a design node  $n$ , the other is to change the material  $m_e$  of a design element  $e$ . A node is a design node  $n$  if it is

- on the surface of the structure,
- not supported,
- not subjected to any external forces and
- not part of a fixed domain (see Section 2.5).

Furthermore, a tetrahedral element is a design element  $e$  if it is

- solid,
- not adjacent to a control point subjected to external forces and
- not part of a fixed domain (see Section 2.5).

For the test cases presented here, we seek to find the structure which is as stiff as possible. Consequently, the objective function is compliance

$$f(\mathbf{m}, \mathbf{p}) = \mathbf{u}^T \mathbf{K}(\mathbf{m}, \mathbf{p}) \mathbf{u} \quad (5)$$

Note that since this objective is a function of the displacements  $\mathbf{u}$ , we need to solve Equation 4 to evaluate it. The reason for choosing to minimize compliance and not for example maximal Von Mises stress is that the compliance function is smooth. This is a significant advantage for the optimization algorithm. However, we plan to minimize the maximal Von Mises stress using the same method in the future.

It is often desirable to constrain the optimization. In some test examples, we choose to limit the amount of

material used, i.e. the optimization is subject to a global volume constraint:

$$g_1(\mathbf{m}, \mathbf{p}) = \frac{V(\mathbf{m}, \mathbf{p})}{V^*} - 1 \quad (6)$$

Where  $V(\mathbf{m}, \mathbf{p})$  is the total volume of the solid elements and  $V^*$  is the maximum volume of the structure.

Optimized results are often not manufacturable. For example, the optimized results often contain many details. A partial remedy is to constrain the total surface area, called a perimeter constraint [42].

$$g_2(\mathbf{m}, \mathbf{p}) = \frac{A(\mathbf{m}, \mathbf{p})}{A^*} - 1 \quad (7)$$

Here,  $A(\mathbf{p})$  is the total area of triangles sandwiched between a void and a (not fixed) solid element and  $A^*$  is the maximum surface area allowed. This constraint enforces a smoothness of the surface and thereby to some degree prevents small details and thin plates. However, since it is a global constraint, these undesirable features are not guaranteed to be eliminated.

Finally, in some cases, we want to limit the possible change from the original shape. In these cases, the original design nodes are added to a set  $O$ . If, during the optimization, an edge connecting two original nodes is split, the new node will be added to the set. However, if a hole appears inside the structure, the nodes on that internal surface are not added. Furthermore, the original surface is stored such that the distance  $d_n(\mathbf{m}, \mathbf{p})$  from  $n \in O$  to the original surface can be calculated. Finally, the function  $t_n(\mathbf{m}, \mathbf{p})$  computes the distance from  $n \notin O$  to the surface represented by the nodes in the set  $O$ . In other words, this function calculates the thickness of the shell of the structure. We can now limit the change from the original surface as well as ensuring that holes will not appear in this surface by applying the constraint:

$$g_3(\mathbf{m}, \mathbf{p}) = \frac{1}{N_{e \in O}} \sum_{n \in O} \max(d_n(\mathbf{m}, \mathbf{p}) - D^*, 0)^2 + \frac{1}{N_{n \notin O}} \sum_{n \notin O} \max(T^* - t_n(\mathbf{m}, \mathbf{p}), 0)^2 \quad (8)$$

Here,  $D^*$  is the maximal change from the original surface and  $T^*$  is the minimum thickness of the shell of the structure. Note that  $g_3$  is  $C^1$  continuous and thereby differentiable.

#### 2.3.1. Continuous optimization

The first part of the optimization procedure is to locally perturb the surface of the structure such that it iteratively gets closer to optimum. This part of the optimization procedure consists of calculating an improved

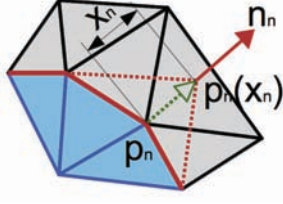


Figure 6: Illustrates the destination  $\mathbf{p}_n(x_n)$  of node  $n$  as a function of the design variable  $x_n$ . Furthermore,  $\mathbf{p}_n$  is the current position and  $\mathbf{n}_n$  is the normal.

400 position  $\mathbf{p}_n^*$  for each design node  $n$ . Afterwards, the  
 401 structure is deformed by moving each design node from  
 402 its current  $\mathbf{p}_n$  to the more optimal position  $\mathbf{p}_n^*$  as de-  
 403 scribed in Section 2.1. Note that since the DSC method  
 404 handles topology changes, these can occur. Thin struc-  
 405 tures can collapse and holes can disappear. However,  
 406 holes will not appear inside the structure during this  
 407 step. Also, note that the material parameter  $\mathbf{m}$  is fixed  
 408 during this step.

409 Moving the design nodes in the tangent directions  
 410 will not change the surface much. Consequently, each  
 411 design node  $n$  is associated with one design variable  
 412 only. A design variable  $x_n$  represents the distance node  $n$   
 413 is moved in the normal direction  $\mathbf{n}_n$  from the current po-  
 414 sition  $\mathbf{p}_n$  as illustrated in Figure 6. The design variables  
 415 are assembled in the vector  $\mathbf{x} = [\dots, x_n, \dots]^T$ . Conse-  
 416 quently, the positions of the control points as a function  
 417 of the design variables can be expressed as  $\mathbf{p}(\mathbf{x})$ .

418 The relation between the current position  $\mathbf{p}_n$ , the op-  
 419 timized position  $\mathbf{p}_n^*$  and the optimized design variable  $x_n^*$   
 420 for a design node  $n$  is

$$\mathbf{p}_n^* = \mathbf{p}_n(x_n^*) = \mathbf{p}_n + x_n^* \mathbf{n}_n \quad (9)$$

421 To estimate  $\mathbf{x}^* = [\dots, x_n^*, \dots]^T$ , a smooth non-linear op-  
 422 timization problem is solved:

$$\begin{aligned} \mathbf{x}^* = \arg \min_{\mathbf{x}} : f(\mathbf{m}, \mathbf{p}(\mathbf{x})) &= \mathbf{u}^T \mathbf{K}(\mathbf{m}, \mathbf{p}(\mathbf{x})) \mathbf{u} \\ \text{subject to} : g_i(\mathbf{m}, \mathbf{p}(\mathbf{x})) &\leq 0, \quad i = 1, 2, 3 \\ &: \mathbf{K}(\mathbf{m}, \mathbf{p}(\mathbf{x})) \mathbf{u} = f(\mathbf{m}, \mathbf{p}(\mathbf{x})) \\ &: \mathbf{x}^{\min} \leq \mathbf{x} \leq \mathbf{x}^{\max} \end{aligned} \quad (10)$$

423 Here,  $\mathbf{x}^{\min} = [\dots, x_n^{\min}, \dots]^T$  and  $\mathbf{x}^{\max} = [\dots, x_n^{\max}, \dots]^T$   
 424 are move limits on the design variables  $\mathbf{x}$ . Generally,  
 425  $\mathbf{x}^{\min}$  and  $\mathbf{x}^{\max}$  are chosen such that the design nodes  
 426 will not create degenerate tetrahedra during the opti-  
 427 mization. Consequently, the new shape can only be a  
 428 small perturbation from the current shape and Equation  
 429 10 will be solved many times. Furthermore, the move

430 limits ensure that the design nodes stay inside a user-  
 431 specified design domain. Therefore, the structure can-  
 432 not extend beyond the boundaries of this design domain.

433 We use the gradient-based optimization algorithm  
 434 Method of Moving Asymptotes (MMA) [14] to solve  
 435 the optimization problem in Equation 10. This is an iter-  
 436 ative optimization procedure which is stopped when the  
 437 infinity norm of the change in  $\mathbf{x}$  is less than a threshold  
 438 or at iteration 5. In addition to evaluating the objective  
 439 function and constraints, the derivatives of these func-  
 440 tions with respect to each of the design variables  $x_n$  have  
 441 to be evaluated at each iteration. Computing  $\frac{\partial}{\partial x_n} \mathbf{u}$  is not  
 442 efficient. However, using the adjoint variable method  
 443 (utilizing the equilibrium equations) [43][44], we get  
 444 an analytical expression for  $\frac{\partial}{\partial x_n} f(\mathbf{m}, \mathbf{p}(\mathbf{x}))$  without the  
 445 problematic term  $\frac{\partial}{\partial x_n} \mathbf{u}$ :

$$\begin{aligned} \frac{\partial f(\mathbf{m}, \mathbf{p}(\mathbf{x}))}{\partial x_n} &= \\ &= -\mathbf{u}^T \frac{\partial \mathbf{K}(\mathbf{m}, \mathbf{p}(\mathbf{x}))}{\partial x_n} \mathbf{u} + 2\mathbf{u}^T \frac{\partial f(\mathbf{m}, \mathbf{p}(\mathbf{x}))}{\partial x_n} \end{aligned} \quad (11)$$

446 Still, since the equilibrium equations have to be evalu-  
 447 ated at each iteration, this continuous optimization step  
 448 is the most expensive part of the optimization proce-  
 449 dure.

### 450 2.3.2. Discrete optimization

451 In addition to changing the shape by moving the de-  
 452 sign nodes, a discrete optimization step is performed  
 453 where the materials  $\mathbf{m}$  are changed and the positions  $\mathbf{p}$   
 454 are not. The step has two purposes; introducing holes  
 455 inside the structure and increasing the convergence rate  
 456 of the continuous optimization. The optimization prob-  
 457 lem can be written as

$$\begin{aligned} \mathbf{m}^* &= \arg \min_{\mathbf{m}} : f(\mathbf{m}, \mathbf{p}) = \mathbf{u}^T \mathbf{K}(\mathbf{m}, \mathbf{p}) \mathbf{u} \\ \text{subject to} : g_i(\mathbf{m}, \mathbf{p}) &\leq 0, \quad i = 1, 2, 3 \\ &: \mathbf{K}(\mathbf{m}, \mathbf{p}) \mathbf{u} = f(\mathbf{m}, \mathbf{p}) \\ &: m_e \in \{\text{void}, \text{solid}\} \end{aligned} \quad (12)$$

458 Note that the set of possible materials is limited to void  
 459 and solid. However, it is possible to extend this ap-  
 460 proach to handle multiple materials. Furthermore, we  
 461 choose that only solid elements are design elements.  
 462 Consequently, this step only removes material from the  
 463 structure. If it removes material near the surface, this  
 464 will speed up shape changes. On the other hand, if it  
 465 removes material inside the structure, a hole is created.

466 The discrete optimization problem in Equation 12 is  
 467 NP-hard. However, since this optimization problem is  
 468 combined with a continuous optimization, it is not nec-  
 469 essary to solve it to optimality. Consequently, this step  
 470 will seek to improve the objective while trying to satisfy  
 471 the constraints by relabeling tetrahedra. The relabeling  
 472 will be based on discrete derivatives, i.e. the change in  
 473 objective or constraints when changing the material in  
 474 element  $e$  from solid to void:

$$\Delta_e f(\mathbf{m}, \mathbf{p}) = f(\mathbf{m}_e^v, \mathbf{p}) - f(\mathbf{m}, \mathbf{p}) \quad (13)$$

$$\Delta_e g_i(\mathbf{m}, \mathbf{p}) = g_i(\mathbf{m}_e^v, \mathbf{p}) - g_i(\mathbf{m}, \mathbf{p}), \quad i = 1, 2, 3 \quad (14)$$

475 Here,  $\mathbf{m}_e^v$  equals  $\mathbf{m}$  where  $m_e$  is void instead of solid.  
 476 However, computing these discrete derivatives for com-  
 477 pliance is inefficient since the equilibrium equations  
 478 then have to be evaluated once for each solid tetrahe-  
 479 dron. Instead, we will use an approximation based on  
 480 the theory of topological derivatives [4][5][45][6]. The  
 481 topological derivative corresponds to the influence on  
 482 the objective function of introducing an infinitesimal  
 483 hole in element  $e$ . For compliance, the discrete deriva-  
 484 tive can therefore be approximated by

$$\Delta_e f(\mathbf{m}, \mathbf{p}) \approx 3\mathbf{u}^T \mathbf{K}_e(\mathbf{m}, \mathbf{p}) \mathbf{u} - \frac{2V_e(\mathbf{p})}{N_{ee}} \sum_{c \in e} \mathbf{u}_c^T \mathbf{g} \quad (15)$$

485 The first part of the optimization strategy is to im-  
 486 prove the objective function while decreasing or satis-  
 487 fying all constraints. A constraint  $i$  is decreased if

$$\Delta_e g_i(\mathbf{m}, \mathbf{p}) \leq 0 \quad (16)$$

488 and satisfied if

$$g_i(\mathbf{m}, \mathbf{p}) + \Delta_e g_i(\mathbf{m}, \mathbf{p}) \leq 0 \quad (17)$$

489 Hence, a design element  $e$  is relabeled from solid to void  
 490 if either of equations 16 and 17 are satisfied for all con-  
 491 straints and

$$\Delta_e f(\mathbf{m}, \mathbf{p}) < 0 \quad (18)$$

492 The second part of the optimization is to try to im-  
 493 prove constraints which are not satisfied. Therefore, if  
 494 constraint  $i$  is not satisfied, i.e.  $g_i(\mathbf{m}, \mathbf{p}) > 0$ , we will  
 495 try to find an optimal design element  $e^*$  to relabel from  
 496 solid to void. Noting that  $\Delta_e f(\mathbf{m}, \mathbf{p}) \geq 0$ , the optimal  
 497 design element  $e^*$  is found by solving

$$e^* = \arg \min_e - \frac{\Delta_e f(\mathbf{m}, \mathbf{p})}{\Delta_e g_i(\mathbf{m}, \mathbf{p})} \quad (19)$$

498 where all arguments  $e$  satisfy

$$\Delta_e g_i(\mathbf{m}, \mathbf{p}) < 0 \quad (20)$$

499 and either Equation 16 or 17 for all constraints. Design  
 500 element  $e^*$  is then relabeled from solid to void. This  
 501 process is repeated as long as constraint  $i$  is not satisfied  
 502 and an optimal element  $e^*$  exists.

#### 503 2.4. Disconnected material

504 The continuous and discrete optimization steps can  
 505 very well result in material which is disconnected from  
 506 the main structure. These parts do not contribute to the  
 507 objective. Furthermore, since void elements are elimi-  
 508 nated from the finite element analysis, disconnected ma-  
 509 terial will result in the equilibrium equations not having  
 510 a unique solution. Consequently, disconnected mate-  
 511 rial is removed by performing a connected component  
 512 analysis and making every component, except for the  
 513 largest, void.

#### 514 2.5. Initialization

515 To initialize the optimization, the user has to specify  
 516 boundary conditions, an objective function, constraints  
 517 and an initial structure.

518 The boundary conditions are the supports and exter-  
 519 nal forces applied to the surface of the structure as de-  
 520 scribed in Section 2.2. Furthermore, the boundaries of  
 521 the design domain (the domain where material can re-  
 522 side) have to be specified. Finally, it is possible to spec-  
 523 ify fixed domains (areas that are either always solid or  
 524 always void). The fixed void areas are implemented as  
 525 not being a part of the design domain. However, the  
 526 fixed solid domains are enforced by assigning a differ-  
 527 ent label to the tetrahedra inside these domains. Con-  
 528 sequently, an invisible surface exists between the fixed  
 529 and non-fixed solid domains. The shape of this surface  
 530 should not be changed in any way. However, we still  
 531 want the DSC method to improve the mesh quality and  
 532 control the level of detail at this surface. Consequently,  
 533 the DSC method is modified such that only mesh oper-  
 534 ations which do not change the surface are performed at  
 535 the surface between fixed and non-fixed domains.

536 In all of the example problems presented here, the ob-  
 537 jective is to minimize compliance since it is often desir-  
 538 able to produce as stiff a structure as possible. However,  
 539 choosing another objective is as simple as changing the  
 540 objective function and calculating the shape and topo-  
 541 logical derivatives of the new function. For example,  
 542 the same approach has been used for balancing of 3D  
 543 models [46]. Furthermore, different problems require  
 544 different constraints. In this paper, we present several  
 545 different global constraints to illustrate their effect on

546 the design. The effect can be quite drastic and conse-  
547 quently the constraints are as important as the objective.

548 Finally, the initial model is a triangle mesh. Conse-  
549 quently, any surface mesh can be used as a starting point  
550 for the optimization without any conversions. In this pa-  
551 per, we choose to initialize the optimization by triangle  
552 meshes of existing models and by generated meshes that  
553 fill the entire design domain.

## 554 2.6. Method summary

555 The method consists of two steps:

### 556 Step 1: Discrete optimization

557 Improves the objective as well as unsatisfied con-  
558 straints by relabeling elements from solid to void  
559 based on their topological derivatives as described  
560 in Section 2.3.2. Then, removes disconnected ma-  
561 terial.

### 562 Step 2: Continuous optimization

563 Solves the optimization problem in Equation 10  
564 using the gradient-based optimization algorithm  
565 MMA (Section 2.3.1). MMA hereby estimates  
566 the optimal values of the design variables  $\mathbf{x}^* =$   
567  $[\dots, x_n^*, \dots]^T$ . Then, each design node  $n$  is moved  
568 from position  $\mathbf{p}_n$  to  $\mathbf{p}_n^* = \mathbf{p}_n + x_n^* \mathbf{n}_n$  using the  
569 DSC method as described in Section 2.1. Finally,  
570 disconnected material is removed.

571 These two steps make up one time step and are iterated  
572 until the changes on the surface from consecutive time  
573 steps are small.

574 Problems can arise if a volume or perimeter con-  
575 straint is applied. The optimization will seek to obey  
576 the constraint before taking the objective into account.  
577 This can lead to undesired removal of material from  
578 places where it is necessary. Our solution to this prob-  
579 lem is to gradually lower the constraint such that  $V^*(t) =$   
580  $\max(\alpha^t, V^*)$  and  $A^*(t) = \max(\beta^t, A^*)$  where  $t$  is the time  
581 step and  $0 < \alpha < 1$  and  $0 < \beta < 1$  are constants.

## 582 2.7. Efficiency

583 Efficiency is essential when performing topology op-  
584 timization in 3D. A major piece of the puzzle to make  
585 this approach more efficient than standard fixed grid  
586 methods is to take advantage of the mesh adaptivity in-  
587 herent to the DSC method. Consequently, the surface is  
588 represented by a fine discretization whereas large tetra-  
589 hedra discretize parts far away from the surface. Fur-  
590 thermore, the main computational power should be used  
591 to achieve a fine resolution near the optimum. When

592 the optimization is initialized by a 3D model, the opti-  
593 mum is assumed to be close. However, that is proba-  
594 bly not the case when the optimization is initialized by  
595 filling the design domain with material. Consequently,  
596 in these cases, we slowly lower the discretization pa-  
597 rameter  $\delta$  by multiplying it by 0.99 at each time step.  
598 The detail control, described in Section 2.1, will then  
599 increase the mesh complexity. Note that this strategy  
600 is especially effective since the method only calculates  
601 on solid elements. However, solving the equilibrium  
602 equations is still the most time-consuming part. Conse-  
603 quently, we utilize multiple threads on the CPU to speed  
604 up these computations. Also, computing the gradients  
605 of the compliance function and assembling the global  
606 stiffness matrix  $K$  and force vector  $F$  are parallelized.

## 607 3. Results

608 The proposed method can be used in the fabrication  
609 design process in areas such as construction, manufac-  
610 turing and design. In this section, we will illustrate  
611 this statement by solving problems within each of these  
612 fields. The results are generated on a laptop with a 2.4  
613 GHz quad-core Intel Core i7 processor and 8 GB of  
614 1333 MHz DDR3 RAM. Parameters and performance  
615 measures are depicted in Table 1. Furthermore, the ob-  
616 jective of all examples is to minimize compliance sub-  
617 ject to constraints as depicted in Table 1.

618 The raw surface triangle meshes of the optimized  
619 structures, i.e. the output as it looks from the optimiza-  
620 tion method, are visualised using Blender. No post pro-  
621 cessing like subdivision and smoothing has been uti-  
622 lized to improve the appearance. Furthermore, when  
623 material has been removed from inside a structure, the  
624 internal cavities are visualized by making the structure  
625 transparent. In addition to the optimized result, we will  
626 in some cases visualize the strain energy density (SED)  
627 at the surface of the final model. The SED depicts how  
628 much strain an element at the surface is subjected to.  
629 Here, the jet colormap is used, where blue and red de-  
630 pict low and high SED respectively. Furthermore, the  
631 SEDs are scaled between the minimum and maximum  
632 SED of the initial structure. Consequently, this visual-  
633 izes how the stiffness has changed as a consequence of  
634 the optimization. In the same cases, we will also visual-  
635 ize the difference from the original model by a grayscale  
636 colormap. Here, gray means no change, darker means it  
637 has moved in the negative normal direction and lighter  
638 that it has moved in the normal direction. The distance  
639 is scaled by the largest change.

Problem	$\delta$	$V^*$ ( $\alpha$ )	$A^*$ ( $\beta$ )	$D^*$	$T^*$	$f^*/f^0$	Surface	Complex	Running time
	mm	% $V^0$ (-)	% $A^0$ (-)	% $\delta$	% $\delta$	-	# faces	# elements	minutes (#)
Bridge	423	20 (0.96)	30 (0.98)	-	-	304 %	9883	29836	68 (70)
Statue	50	50 (0.95)	-	15	100	27 %	35868	66314	275 (20)
Dinosaur	1.4	-	-	15	100	46 %	6876	15071	11 (5)
Armadillo	2.8	-	-	15	100	13 %	9872	15819	60 (50)
Table 1	42	15 (0.96)	30 (0.98)	-	-	2671 %	5492	11761	16 (100)
Table 2	62	15 (0.96)	35 (0.98)	-	-	964 %	3543	5521	13 (60)
Table 3	42	15 (0.96)	30 (0.98)	-	-	5929 %	5374	11759	20 (100)
Chair 1	21	12.5 (0.96)	25 (0.98)	-	-	1199 %	4413	7929	15 (100)
Chair 2	21	12.5 (0.96)	30 (0.98)	-	-	625 %	5527	9026	18 (100)
Chair 3	27	12.5 (0.96)	30 (0.98)	-	-	927 %	3382	4927	8 (75)
Support	655	20 (0.96)	20 (0.98)	-	-	17 %	15064	27120	109 (100)

Table 1: Method parameters and performance measures for all example problems. The displayed values are the values as they appear after the optimization. The  $V^*$  and  $A^*$  values are stated in percent of the initial volume  $V^0$  and surface area  $A^0$  respectively whereas  $D^*$  and  $T^*$  are stated in percent of the discretization parameter  $\delta$ . Furthermore,  $f^0$  and  $f^*$  are initial and final compliance respectively. Finally, the # in the right-most column is the number of time steps.

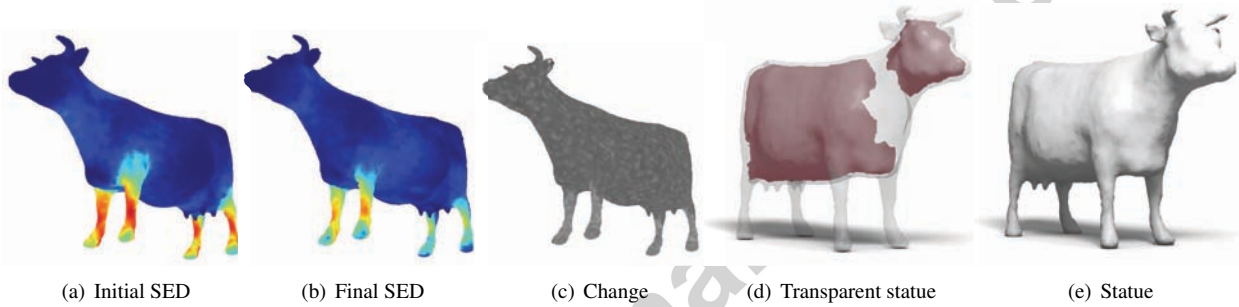


Figure 7: Topology optimized cow statue which show that the method can optimize stiffness while saving material.

### 640 3.1. Construction

641 Topology optimization has traditionally been used  
642 for construction where the objective is to save material  
643 while ensuring stiffness. The presented method has the  
644 same capabilities as previous methods. Furthermore, it  
645 extends those methods by being able to initialize an op-  
646 timization by a surface triangle mesh with no conversion  
647 necessary.

648 First, a bridge problem is initialized by a steel cube  
649 ( $30 \times 15 \times 12 \text{ m}^3$ ) with a space for vehicles and supports  
650 as depicted in Figure 1. The surface of the bridge is  
651 fixed and subjected to a distributed load pushing down-  
652 wards (100 MPa). The result and optimization process  
653 are also depicted in Figure 1. The result shows that com-  
654 pliance has increased to 304% of the initial value during  
655 the optimization process. However, the optimized struc-  
656 ture only uses 20% of the material used by the initial  
657 structure.

658 Next, a 4 m-long concrete statue is initialized by a  
659 3D model of a cow (source: Aim@Shape). The statue

660 is solid concrete, only subjected to gravitational forces  
661 and supported underneath all of its hoofs. The change  
662 in SED, shape changes and the optimized cow statue  
663 are depicted in Figure 7. This example shows that our  
664 method extends previous methods by being able to ini-  
665 tialize an optimization by a 3D model (represented by  
666 a triangle mesh) without any conversion and, further-  
667 more, remain close to this shape. Also, since the statue  
668 is subjected to gravitational forces only, compliance is  
669 improved at the same time as the amount of material is  
670 reduced.

### 671 3.2. Manufacturing

672 An important application of our method is as a tool to  
673 improve the stiffness of a given shape. Assume, we are  
674 given a 3D shape that is to be fabricated. The problem  
675 is to change the exterior shape as little as possible while  
676 using a minimum amount of material and ensuring that  
677 the fabricated object will be able to support itself and  
678 moreover withstand specified external loads. Further-

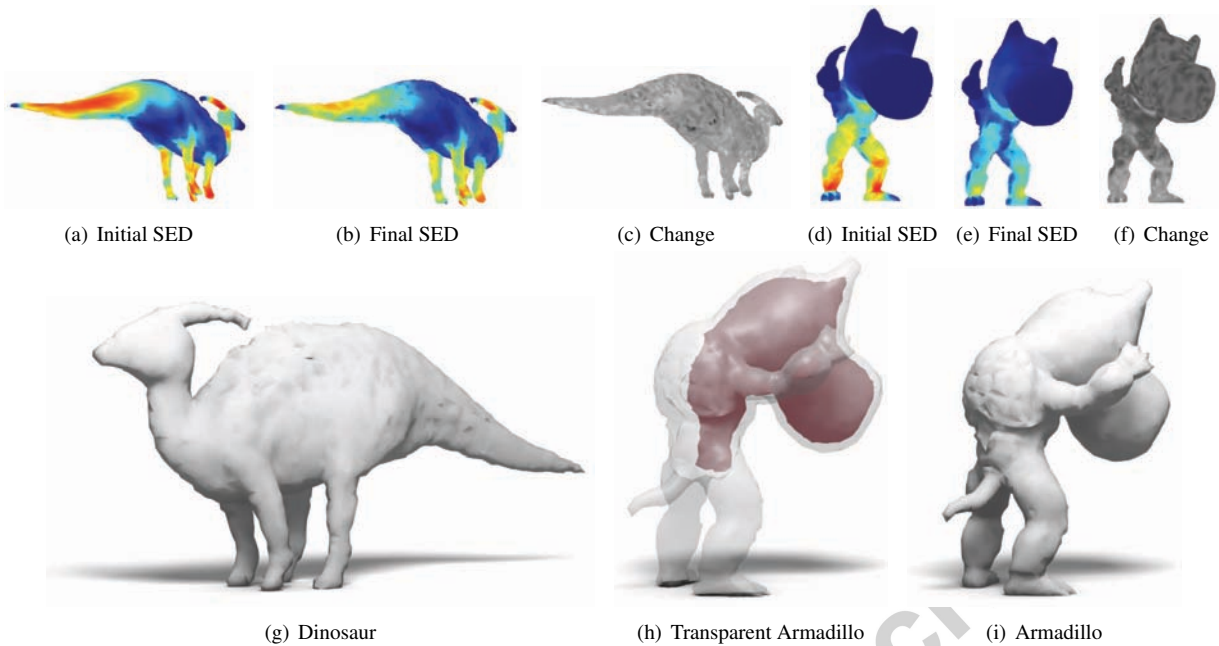


Figure 8: Toy models optimized to improve both stiffness and balance while remaining close to the initial shape.

679 more, a side effect of optimizing a structure to bear its  
680 own weight is that the balance is improved.

681 A 10 cm-long plastic model of a dinosaur (source:  
682 Aim@Shape) is subjected to external forces (5 MPa)  
683 on the tail and the head where one would expect the  
684 model to be weakest. Furthermore, each of the four feet  
685 are supported. The SEDs, shape changes and optimized  
686 dinosaur are depicted in Figure 8. Since the external  
687 forces are large compared to the gravitational forces,  
688 the optimization does not create any cavities. Instead, it  
689 redistributes material to places where it improves stiff-  
690 ness. Consequently, compliance is minimized to 46%  
691 of the initial value.

692 Next, a 10 cm-high plastic Armadillo model with  
693 a large head (source: Stanford University Computer  
694 Graphics Laboratory and edited in MeshMixer) is sup-  
695 ported underneath both feet and only subject to gravity.  
696 The SEDs, shape changes and optimized model can be  
697 seen in Figure 8. It is evident that since the model has  
698 a large head it will lean forward and thereby subject the  
699 shins to large strain. When optimizing compliance, the  
700 strain is minimized and the balance of the model is im-  
701 proved as a side effect. However, since imbalance is not  
702 directly penalized by the objective function, balance is  
703 not guaranteed. A modification of the objective function  
704 or constraints would, however, guarantee balance by re-  
705 quiring the center of gravity to stay within the convex

706 hull of the supports.

### 707 3.3. Design

708 When humans design a given 3D object, the main  
709 concerns are often to satisfy aesthetic and functional  
710 requirements. Topology optimization is not concerned  
711 with aesthetics but it satisfies functional requirements.  
712 However, topology-optimized shapes exhibit an organic  
713 and sparse feeling that is often visually pleasing. There-  
714 fore, such a tool is useful as part of a design workflow  
715 [47]. Furthermore, the method can be used to generate  
716 significantly different designs by slight changes to the  
717 input. This is significantly simpler for a designer than  
718 remodeling a surface.

719 Three plastic tables are modeled by a fixed layer of  
720 material at the top of a design domain (1.8 1.2 1.2  
721 m<sup>3</sup>) and a distributed load (2 MPa) pressing down on  
722 this layer. Furthermore, three chairs are initialized by  
723 filling a 0.6 0.8 0.6 m<sup>3</sup> design domain. The seat is  
724 modeled by a fixed void domain of size 0.4 0.4 0.4 m<sup>3</sup>  
725 and a fixed solid domain underneath which is subjected  
726 to a load (1 MPa). Finally, a backrest is modeled by a  
727 small fixed solid domain and subjected to a horizontal  
728 force (0.5 MPa). The difference between the problems  
729 are the position and extent of the supports. All supports  
730 are placed at the bottom of the design domain and have  
731 the shape depicted in figures 9(a), 9(d) and 9(g) as seen

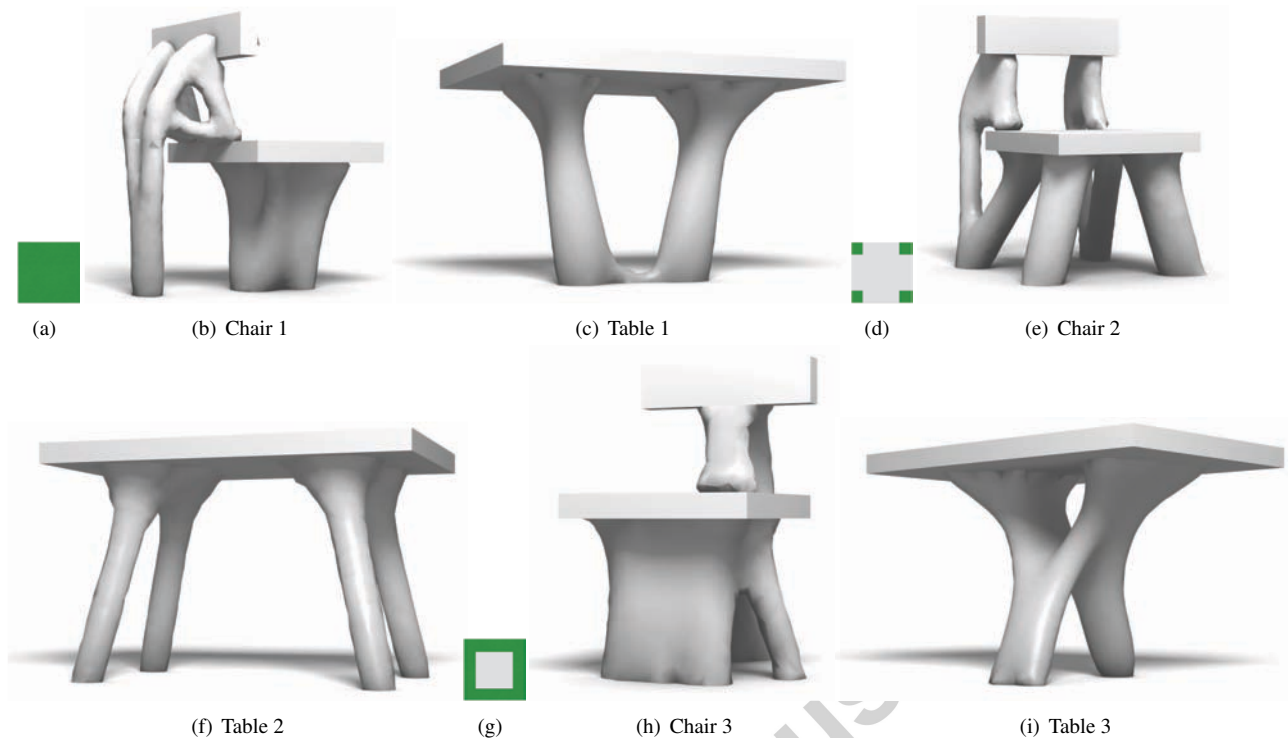


Figure 9: Topology optimized tables and chairs which show the design capabilities of the suggested method. The difference between the problems are the supports (illustrated at the left of each row) and possibly the values of parameters. Note that the same illustration is used for both a table and a chair problem, therefore the dimensions of these illustrations are not correct.

732 from above. The optimized designs are depicted in Fig-  
733 ure 9.

734 Finally, we will use the Qatar National Convention  
735 Center as an example of a real-world architectural de-  
736 sign problem. The Convention Center has an impressive  
737 façade which is a roof supported by a concrete topology-  
738 optimized structure [47]. To model this, we take advan-  
739 tage of the symmetry and thereby only optimize a quar-  
740 ter of the structure (the symmetry axes are depicted in  
741 Figure 10(d)). Consequently, the problem is initialized  
742 by a  $125 \times 20 \times 15 \text{ m}^3$  cube where the top layer (1 m) is  
743 fixed and solid. The structure is supported at the bottom  
744 in a half circular area (Figure 10(d)) and only subjected  
745 to gravity. The result can be seen in Figure 10(e) and, in  
746 addition, we illustrate in Figure 10 the effect of chang-  
747 ing the parameter for the perimeter constraint. Note that  
748 the result is not expected to look like the Convention  
749 Center since [47] use different boundary conditions and  
750 do not specify material, objective and constraints.

#### 751 4. Conclusion

752 The presented method is the first to optimize both  
753 the 3D shape and topology of a surface triangle mesh  
754 without the use of an implicit representation. This is  
755 achieved by embedding the triangle mesh in a simplicial  
756 complex and using the Deformable Simplicial Complex  
757 method. Consequently, the method accepts a surface tri-  
758 angle mesh as input and outputs another surface triangle  
759 mesh which is only different from the input mesh where  
760 it has been optimized. Furthermore, as opposed to stan-  
761 dard fixed grid methods, our method makes it possible  
762 to generate detailed designs within reasonable time on  
763 an ordinary laptop.

764 We have shown that the method automatically gener-  
765 ates designs which satisfy some user-defined structural  
766 requirements. However, note that the search space is  
767 limited by global constraints and that there is no guaran-  
768 tee that the global optimum is reached. The bridge and  
769 the cow statue show that material can be saved where it  
770 is expensive or inconvenient while maintaining or im-  
771 proving stiffness. The dinosaur and Armadillo models  
772 show that 3D models automatically can be made stiffer

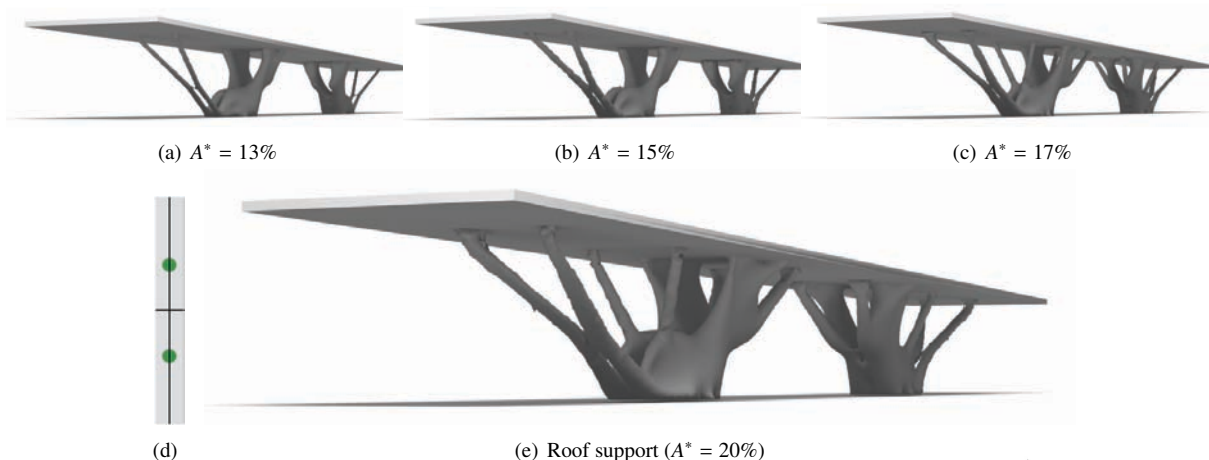


Figure 10: Topology optimized roof support, optimized using different values for the perimeter constraint. This problem is inspired by the real world problem of supporting the roof of the Qatar National Convention Center. The supports are placed as depicted in Figure 10(d) where also symmetry axes are visualized as black lines.

773 and more balanced, while retaining the shape. Finally,  
 774 the tables, chairs and roof support show that functional  
 775 and, in our opinion, visually pleasing designs can be  
 776 achieved with little effort from a designer. This is far  
 777 from an exhaustive list of problems that can be solved  
 778 using the presented method. As mentioned, topology  
 779 optimization has been used to solve a wide variety of  
 780 problems. To solve these or other problems, one only  
 781 needs to model the boundary conditions and choose the  
 782 objective, constraints and an initial structure. How-  
 783 ever, more advanced problems might require additional  
 784 work. For example implementing additional objective  
 785 functions and constraints, handling multiple load cases,  
 786 using an anisotropic material model, handling dynamic  
 787 problems and taking non-linearity into account.

788 We have shown that furniture and support structures  
 789 for buildings can be modeled by specifying a few in-  
 790 put parameters. Furthermore, both the input and output  
 791 models are in the form of a surface triangle mesh. Con-  
 792 sequently, this tool has potential to be used for model-  
 793 ing for films, videogames and other offline productions  
 794 in addition to designing physical structures, especially  
 795 if performance and user friendliness are improved. To  
 796 increase performance, one idea is to take full advan-  
 797 tage of the parallel nature of the finite element compu-  
 798 tations by, for example, feeding the computations to the  
 799 GPU. Furthermore, parallelization of the DSC method  
 800 would be beneficial. Another idea is to take even fur-  
 801 ther advantage of the mesh adaptivity by lowering the  
 802 discretization parameter more wisely. To increase the  
 803 user friendliness, automatic determination of worst-case

804 loads could be useful to limit the amount of user input.  
 805 Also, finding an alternative to the perimeter constraint  
 806 would be desirable since it can limit the optimization  
 807 and its parameter is unintuitive and difficult to choose.  
 808 Finally, most designers want to influence the design reg-  
 809 ularly during the design process. Therefore, a work-  
 810 flow which includes user feedback and post processing  
 811 is needed.

## 812 Acknowledgements

813 The authors appreciate the support from the Villum  
 814 Foundation through the grant: "NextTop"

- 815 [1] M. P. Bendsøe, N. Kikuchi, Generating optimal topologies in  
 816 structural design using a homogenization method, *Computer  
 817 Methods in Applied Mechanics and Engineering* 71 (2) (1988)  
 818 197 – 224.  
 819 [2] M. P. Bendsøe, O. Sigmund, *Topology Optimization - Theory,  
 820 Methods, and Applications*, second edition Edition, Springer  
 821 Verlag, Berlin, 2003.  
 822 [3] M. K. Misztal, J. A. Bærentzen, Topology adaptive interface  
 823 tracking using the deformable simplicial complex, *ACM Trans-  
 824 actions on Graphics* 31 (3) (2012) No. 24.  
 825 [4] H. A. Eschenauer, V. V. Kobelev, A. Schumacher, Bubble  
 826 method for topology and shape optimization of structures, *Struc-  
 827 tural and Multidisciplinary Optimization* 8 (1994) 42–51.  
 828 [5] J. Sokolowski, A. Zochowski, On the topological derivative in  
 829 shape optimization, *SIAM Journal on Control and Optimization*  
 830 37 (4) (1999) 1251–1272.  
 831 [6] R. A. Feijóo, A. A. Novotny, E. Taroco, C. Padra, The topolog-  
 832 ical derivative for the poisson's problem, *Mathematical Models  
 833 and Methods in Applied Sciences* 13 (12) (2003) 1825–1844.  
 834 [7] S. Garreau, P. Guillaume, M. Masmoudi, The topological  
 835 asymptotic for pde systems: The elasticity case, *SIAM J. Con-  
 836 trol Optim.* 39 (6) (2000) 1756–1778.

- 837 [8] F. de Gournay, G. Allaire, F. Jouve, Shape and topology optimization of the robust compliance via the level set method, *ESAIM: Control, Optimisation and Calculus of Variations* 14 (2008) 43–70.
- 838
- 839
- 840
- 841 [9] C. Le, T. Bruns, D. Tortorelli, A gradient-based, parameter-free approach to shape optimization, *Computer Methods in Applied Mechanics and Engineering* 200 (9-12) (2011) 985–996.
- 842
- 843
- 844 [10] S. Arnout, M. Firl, K.-U. Bletzinger, Parameter free shape and thickness optimisation considering stress response, *Structural and Multidisciplinary Optimization* 45 (6) (2012) 801–814.
- 845
- 846
- 847 [11] Y. Ding, Shape optimization of structures: a literature survey, *Computers & Structures* 24 (6) (1986) 985–1004.
- 848
- 849 [12] B. Mohammadi, F. O. Pironneau, *Applied Shape Optimization for Fluids*, Oxford University Press, 2009.
- 850
- 851 [13] D. Bucur, G. Buttazzo, *Variational Methods in Shape Optimization Problems*, Progress in Nonlinear Differential Equations and Their Applications, Birkhäuser, 2006.
- 852
- 853
- 854 [14] K. Svanberg, The method of moving asymptotes – a new method for structural optimization, *International Journal for Numerical Methods in Engineering* 24 (2) (1987) 359–373.
- 855
- 856
- 857 [15] R. Prévost, E. Whiting, S. Lefebvre, O. Sorkine-Hornung, Make It Stand: Balancing shapes for 3D fabrication, *ACM Transactions on Graphics (proceedings of ACM SIGGRAPH)* 32 (4) (2013) 81:1–81:10.
- 858
- 859
- 860
- 861 [16] M. Skouras, B. Thomaszewski, S. Coros, B. Bickel, M. Gross, Computational design of actuated deformable characters, *ACM Trans. Graph.* 32 (4) (2013) 82:1–82:10.
- 862
- 863
- 864 [17] F. De Goes, P. Alliez, H. Owahdi, M. Desbrun, On the Equilibrium of Simplicial Masonry Structures, *ACM Transactions on Graphics* 32 (4).
- 865
- 866
- 867 [18] Y. Liu, H. Pan, J. Snyder, W. Wang, B. Guo, Computing self-supporting surfaces by regular triangulation, *ACM Trans. Graph.* 32 (4) (2013) 92:1–92:10.
- 868
- 869
- 870 [19] D. Panozzo, P. Block, O. Sorkine-Hornung, Designing unreinforced masonry models, *ACM Transactions on Graphics (proceedings of ACM SIGGRAPH)* 32 (4) (2013) 91:1–91:12.
- 871
- 872
- 873 [20] N. Umetani, R. Schmidt, Cross-sectional structural analysis for 3d printing optimization, in: *SIGGRAPH Asia 2013 Technical Briefs*, SA '13, ACM, New York, NY, USA, 2013, pp. 5:1–5:04.
- 874
- 875
- 876 [21] O. Stava, J. Vanek, B. Benes, N. Carr, R. Mech, Stress relief: Improving structural strength of 3d printable objects, *ACM Trans. Graph.* 31 (4) (2012) 48:1–48:11.
- 877
- 878
- 879 [22] Q. Zhou, J. Panetta, D. Zorin, Worst-case structural analysis, *ACM Trans. Graph.* 32 (4) (2013) 137:1–137:12.
- 880
- 881 [23] M. P. Bendsøe, Optimal shape design as a material distribution problem, *Structural Optimization* 1 (4) (1989) 193–202.
- 882
- 883 [24] S. J. Osher, R. P. Fedkiw, *Level Set Methods and Dynamic Implicit Surfaces*, 1st Edition, Springer, 2002.
- 884
- 885 [25] M. Wang, X. Wang, D. Guo, A level set method for structural topology optimization, *Computer Methods in Applied Mechanics and Engineering* 192 (1) (2003) 227–246.
- 886
- 887
- 888 [26] G. Allaire, F. Jouve, A.-M. Toader, Structural optimization using sensitivity analysis and a level-set method, *Journal of Computational Physics* 194 (1) (2004) 363–393.
- 889
- 890
- 891 [27] S.-H. Ha, S. Cho, Level set based topological shape optimization of geometrically nonlinear structures using unstructured mesh, *Computers & Structures* 86 (13-14) (2008) 1447–1455.
- 892
- 893
- 894 [28] G. Allaire, C. Dapogny, P. Frey, Topology and geometry optimization of elastic structures by exact deformation of simplicial mesh, *Comptes Rendus Mathématique* 349 (17-18) (2011) 999–1003.
- 895
- 896
- 897
- 898 [29] S. Yamasaki, T. Nomura, A. Kawamoto, K. Sato, S. Nishiwaki, A level set-based topology optimization method targeting metallic waveguide design problems, *International Journal for Numerical Methods in Engineering* 87 (9) (2011) 844–868.
- 899
- 900
- 901
- 902 [30] Q. Xia, T. Shi, S. Liu, M. Y. Wang, A level set solution to the stress-based structural shape and topology optimization, *Computers & Structures* 90 - 91 (0) (2012) 55–64.
- 903
- 904
- 905 [31] G. Allaire, C. Dapogny, P. Frey, A mesh evolution algorithm based on the level set method for geometry and topology optimization, *Structural and Multidisciplinary Optimization* 48 (4) (2013) 711–715.
- 906
- 907
- 908
- 909 [32] K. Maute, E. Ramm, Adaptive topology optimization, *Structural optimization* 10 (1995) 100–112.
- 910
- 911 [33] A. N. Christiansen, M. Nobel-Jørgensen, N. Aage, O. Sigmund, J. A. Bærentzen, Topology optimization using an explicit interface representation, *Structural and Multidisciplinary Optimization* 49 (3) (2014) 387–399.
- 912
- 913
- 914
- 915 [34] H. Si, TetGen: A quality tetrahedral mesh generator and a 3d delaunay triangulator (2013).
- 916
- 917 URL <http://wias-berlin.de/software/tetgen/>
- 918 [35] V. N. Parthasarathy, C. M. Graichen, A. F. Hathaway, A comparison of tetrahedron quality measures, *Finite Elem. Anal. Des.* 15 (3) (1994) 255–261.
- 919
- 920
- 921 [36] D. A. Field, Laplacian smoothing and delaunay triangulations, *Communications in Applied Numerical Methods* 4 (6) (1988) 709–712.
- 922
- 923
- 924 [37] J. A. Bærentzen, J. Gravesen, F. Anton, H. Aanæs, Guide to Computational Geometry Processing: Foundations, Algorithms, and Methods, Springer, 2012.
- 925
- 926
- 927 [38] J. R. Shewchuk, Two discrete optimization algorithms for the topological improvement of tetrahedral meshes, in: *Unpublished manuscript*, 2002.
- 928
- 929
- 930 [39] R. D. Cook, D. S. Malkus, M. E. Plesha, R. J. Witt, *Concepts and Applications of Finite Element Analysis*, John Wiley & Sons, 2007.
- 931
- 932
- 933 [40] Y. Chen, T. A. Davis, W. W. Hager, S. Rajamanickam, Algorithm 887: Cholmod, supernodal sparse cholesky factorization and update/downdate, *ACM Transactions on Mathematical Software* 35 (3) (2008) 22:1–22:14.
- 934
- 935
- 936
- 937 [41] T. A. Davis, W. W. Hager, I. S. Duff, SuiteSparse (2013).
- 938
- 939 URL <http://www.cise.ufl.edu/research/sparse/SuiteSparse/>
- 940 [42] R. Haber, C. Jog, M. Bendsøe, A new approach to variable-topology shape design using a constraint on perimeter, *Structural optimization* 11 (1-2) (1996) 1–12.
- 941
- 942
- 943 [43] O. Pironneau, Optimal shape design for elliptic systems, in: R. Drenick, F. Kozin (Eds.), *System Modeling and Optimization*, Vol. 38 of Lecture Notes in Control and Information Sciences, Springer Berlin Heidelberg, 1982, pp. 42–66.
- 944
- 945
- 946 [44] P. W. Christensen, A. Klarbring, *An Introduction to Structural Optimization, Solid mechanics and its applications*, Springer, 2008.
- 947
- 948
- 949
- 950 [45] J. Céa, S. Garreau, P. Guillaume, M. Masmoudi, The shape and topological optimizations connection, *Computer Methods in Applied Mechanics and Engineering* 188 (4) (2000) 713–726.
- 951
- 952
- 953 [46] A. N. Christiansen, R. Schmidt, J. A. Bærentzen, Automatic balancing of 3d models, *Computer-Aided Design* (2014) to appear.
- 954
- 955 [47] M. Sasaki, T. Itō, A. Isozaki, *Morphogenesis of flux structure*, AA Publications, 2007.
- 956